Physica A 479 (2017) 279–286

Contents lists available at ScienceDirect

Physica A

journal homepage: www.elsevier.com/locate/physa

Learning and retrieval behavior in recurrent neural networks with pre-synaptic dependent homeostatic plasticity

Beatriz E.P. Mizusaki [a,*], Everton J. Agnes [a,b], Rubem Erichsen Jr. [a], Leonardo G. Brunnet [a]

[a] Instituto de Física, Universidade Federal do Rio Grande do Sul, Av. Bento Gonçalves, 9500, P.B. 15051, 91501-970 Porto Alegre, Brazil
[b] Centre for Neural Circuits and Behaviour, University of Oxford, Tinsley Building, Mansfield Road, Oxford OX1 3SR, UK

HIGHLIGHTS

- A network of spiking neurons is capable of storing spatio-temporal information.
- A correlation measure to evaluate the quality of the memory retrieved is proposed.
- The storage capacity is evaluated for varied durations of activity traces.
- The time length of inhibitory signals affect the reliability of memory retrieval.

ARTICLE INFO

Article history:
Received 20 September 2016
Received in revised form 11 January 2017
Available online 28 February 2017

Keywords:
Synaptic plasticity
Spike pattern
Spike timing
Recurrent network
Homeostatic plasticity

ABSTRACT

The plastic character of brain synapses is considered to be one of the foundations for the formation of memories. There are numerous kinds of such phenomenon currently described in the literature, but their role in the development of information pathways in neural networks with recurrent architectures is still not completely clear. In this paper we study the role of an activity-based process, called pre-synaptic dependent homeostatic scaling, in the organization of networks that yield precise-timed spiking patterns. It encodes spatio-temporal information in the synaptic weights as it associates a learned input with a specific response. We introduce a correlation measure to evaluate the precision of the spiking patterns and explore the effects of different inhibitory interactions and learning parameters. We find that large learning periods are important in order to improve the network learning capacity and discuss this ability in the presence of distinct inhibitory currents.

1. Introduction

Time intervals between action potentials are frequently regarded as possible information carriers for neural processing [1–3]. In another way there is rate coding, in which the main idea is that groups of neurons, so-called cell assemblies, encode the information. Recent theoretical works have furthered our understanding on the mechanisms necessary to form and retrieve memories as spiking cell assemblies [4–6] and on the storage capacity of these networks [7].

Several experimental studies report the detection of precisely timed patterns of neuronal action potentials, specially in the visual [8] and auditory cortices [9,10], suggesting that information can be represented by the time intervals between spikes[1]. Although this is a controversial subject [11,12], the precise spiking times of a neural population are clear candidates

* Corresponding author.
E-mail address: beatriz@if.ufrgs.br (B.E.P. Mizusaki).

http://dx.doi.org/10.1016/j.physa.2017.02.035
0378-4371/

to be carriers of information. This has been successfully explored in the context of feedforward neural networks [1,13,14]; however, when recurrent connections are considered, a satisfactory model has yet to be achieved. Even though many have been proposed, employing mechanisms such as axonal delay [15], network architecture [16] or synaptic plasticity [17–23], there is always the issue of stability and overwriting.

Liu and co-workers [24,25] explored a plasticity mechanism that is a modified version of homeostatic synaptic scaling (HSS) [26,27], called pre-synaptic dependent scaling (PSD) [28]. HSS is an experimentally observed phenomenon that is considered to be a tuning instrument for the basal activity of each neuron [26,29]. Nevertheless, it is argued that in its most simple proposed formulation [27] it is prone to instabilities such as synfire explosions and oscillations[28,30]. PSD counters the whole cell aspect of HSS with the introduction of a local dependence to the plasticity of the synapses, with each site evolving independently from its neighbors, regulated by both pre and post-synaptic activities. As it also introduces an anti-Hebbian character that is not original from the HSS, one might guess that it presents different computational consequences. In fact, Liu and co-workers report that its presence results in a selective network that gives different responses for input patterns even if only slightly mismatched [25]. This means that, whilst aiming to keep the homeostatic firing rate, it also learns to recognize external inputs [24].

In this work, we describe the properties of a neural network under PSD by introducing a correlation measure to quantify both reliability and precision [8] of the action potential times. This enables the overall network dynamics to be monitored, and the number of different inputs the network can learn to associate with an unique response to be estimated. In order to avoid the possibility that a neuron could spike after a single presynaptic spike, a limit to the synaptic weights can be imposed on the learning rule. The simulated network and its activity are described in Sections 2 and 3, respectively, and Section 4 details the measurement we used to quantify pattern learning. In Section 5 we show the results of limited and unlimited rules over the weight distributions and also that the coupling parameter between the activity and the plasticity, α_A, governs a transition between two distinct pattern retrieval behaviors. Finally, in Section 6, we show that manipulation of the decay times of inhibitory synaptic currents can enhance the network performance.

2. Neural dynamics model

We used the model proposed by Izhikevich [31] to simulate the dynamics of each neuron. The time evolution of the membrane potential of the ith neuron, $v_i(t)$, is described by

$$C\frac{dv_i(t)}{dt} = k\big(v_i(t) - v_r\big)\big(v_i(t) - v_t\big) - u_i(t) - I_i(t)\,, \tag{1}$$

where $u_i(t)$ is a recovery variable whose dynamics is given by

$$\frac{du_i(t)}{dt} = a\big[b\big(v_i(t) - v_r\big) - u_i(t)\big]. \tag{2}$$

The total current input to the neuron is

$$I_i(t) = I_i^{ext}(t) + I_i^{syn}(t)\,. \tag{3}$$

A condition is imposed to signalize the occurrence of a spike:

$$\text{if } v_i(t) \geq v_{peak},\ \begin{cases} v_i(t) \leftarrow c \\ u_i(t) \leftarrow u_i(t) + d. \end{cases} \tag{4}$$

The parameter values are set to $a = 0.01\ \text{ms}^{-1}, b = 5\ \mu\text{S}, c = -60\ \text{mV}, d = 400\ \text{pA}, C = 100\ \text{pF}, v_r = -60\ \text{mV}, v_t = -50\ \text{mV}$, $v_{peak} = 50\ \text{mV}$, and $k = 3\ \mu\text{S/mV}$, for excitatory neurons, and $a = 0.15\ \text{ms}^{-1}$, $b = 8\ \mu\text{S}$, $c = -55\ \text{mV}$, $d = 200\ \text{pA}$, $C = 20\ \text{pF}$, $v_r = -55\ \text{mV}$, $v_t = -40\ \text{mV}$, $v_{peak} = 25\ \text{mV}$, and $k = 3\ \mu\text{S/mV}$, for inhibitory neurons. They are adjusted so that the model neurons may display a behavior that is compatible with pyramidal neurons and interneurons, following regular-spiking (RS) and fast-spiking (FS) activity regimes respectively, as described in Ref. [32]. The equations were integrated by the Euler method with a time step of 1 ms for all variables except for $v_i(t)$, which was integrated with a 0.5 ms step. The amplitude of $I_i^{syn}(t)$ follows four (except in Fig. 4, in which this is varied) time-varying membrane conductances $g^R(t)$, controlled by $R-$type receptors of the post-synaptic neuron [33]. These are the excitatory α-amino-3-hydroxy-5-methyl-4-isoxazolepropionic acid receptor (AMPA) and N-methyl-D-aspartate (NMDA) receptor and the inhibitory γ-aminobutyric acid (GABA) receptors GABA_A and GABA_B. The synaptic current is given by

$$I_i^{syn}(t) = g_i^{AMPA}(t)v_i(t) + g_i^{GABA_A}(t)\big(v_i(t) + 70\ \text{mV}\big) + g_i^{NMDA}(t)h(v_i)v_i(t) + g_i^{GABA_B}(t)\big(v_i(t) + 90\ \text{mV}\big), \tag{5}$$

with $h(v)$ representing the effect of the magnesium (Mg^{2+}) block at NMDA channels,

$$h(v) = \left(\frac{v + 80\ \text{mV}}{60\ \text{mV}}\right)^2\left[1 + \left(\frac{v + 80\ \text{mV}}{60\ \text{mV}}\right)^2\right]^{-1}. \tag{6}$$

The conductances evolve according to the general equation

$$\frac{dg_i^R(t)}{dt} = -\frac{g_i^R(t)}{\tau_R}, \tag{7}$$

decaying exponentially to zero unless there is a presynaptic action potential. When a spike is detected by the post-synaptic neuron i, the term $W_{ij}^T x_j(t)$ is added to the amplitude of each sub-component g^R. The weight of the connection from neuron j to i is represented by W_{ij}^T, where the index T represents the trial (explained below). The term $x_j(t)$ scales the effective weight due to short-term plasticity (detailed below). Thus,

$$g_i^R(t) \leftarrow g_i^R(t) + W_{ij}^T x_j(t)\,, \tag{8}$$

if the neuron j fired on time $t - \Delta$. The time decay constants are $\tau_{AMPA} = 5$ ms, $\tau_{NMDA} = 150$ ms, $\tau_{GABA_A} = 6$ ms and $\tau_{GABA_B} = 150$ ms. The fixed axonal transmission delays, Δ, are 1 ms and 2 ms in excitatory and inhibitory connections, respectively.

Network parameters

The networks simulated in the present work are composed of $N = 500$ neurons, 80% of which are excitatory ($N_e = 400$) and 20% inhibitory ($N_i = 100$). The number of synapses between pairs of pre and post-synaptic neurons is determined according to the network size: $0.12\,N_e$ excitatory and $0.2\,N_i$ inhibitory connections arrive at each excitatory neuron and $0.2\,N_e$ excitatory connections arrive at each inhibitory neuron. There are no direct connections between inhibitory neurons. The synaptic matrix is randomly sorted, respecting the values mentioned above, and a small initial weight value is assigned to each connection: $W_{exc\to exc} = 0.2$ nS for a connection between two excitatory neurons, $W_{exc\to inh} = 0.04$ nS for a connection from an excitatory neuron to an inhibitory one and $W_{inh\to exc} = 0.4$ nS for a connection from an inhibitory neuron to an excitatory one, except when noted.

Synaptic plasticity

The synaptic weight from the pre-synaptic neuron j to the post-synaptic neuron i, W_{ij}, is modified in a discrete event time scheme, as in Ref. [28]. A trial is defined as a block of time consisting of an initial spike pattern evoked on the network and the subsequent transient activity; the synaptic weights are updated after it ends. Each pattern is composed of a group of 7% of the network neurons driven synchronously to the spiking threshold. The initial configuration of $W_{ij}^{T=1}$ and $v_i(t = 0)$ is arranged so that the network remains in a quiescent state unless there is an external input. A long-term plasticity mechanism shapes the excitatory synapses: the pre-synaptic-dependent homeostatic synaptic scaling (PSD). Inhibitory synapses do not change during the simulations.

We consider homeostatic synaptic scaling [27] with a multiplicative dependence on the activity of the pre-synaptic neuron j, as proposed in Ref. [28] and called PSD. The weight values evolve according to

$$W_{ij}^{T+1} = W_{ij}^T + \alpha_W A_j^T \left(A_{goal} - A_i^T\right) W_{ij}^T\,, \tag{9}$$

where T is the trial index and A_i^T is an accumulated medium value for the number of spikes S_i^T fired by the neuron i in trial T. A_i^T evolves as

$$A_i^{T+1} = A_i^T + \alpha_A \left(S_i^T - A_i^T\right). \tag{10}$$

The growth rates for W_{ij}^T and A_i^T are determined by $\alpha_W = 0.01$ and $\alpha_A = 0.05$, respectively, except in the last panel of Fig. 3(b), in which $\alpha_A = 1$. A_{goal} is the target activity per neuron, which is set to 1 and 2 spikes per trial for excitatory and inhibitory neurons, respectively. The weight growth is halted if it reaches a maximum value $W_{exc\to exc}^{max} = 1.5$ nS or $W_{exc\to ini}^{max} = 0.45$ nS, with hard bounds. Some simulations were performed with unbounded weights which were indicated in the labels. This is to avoid the possibility of a single synapse getting big enough to independently excite a post-synaptic spike as well as positive-feedback issues [34].

We implemented short-term depression (STD) as in Ref. [32], introducing an auxiliary variable $x_j(t)$ to modulate the synaptic weight W_{ij}, according to the activity of the presynaptic neuron j. In the absence of pre-synaptic spikes, $x_j(t)$ evolves towards one with dynamics given by

$$\frac{dx_j(t)}{dt} = \frac{1 - x_j(t)}{\tau_x}. \tag{11}$$

When the presynaptic neuron j fires an action potential the auxiliary variable is scaled by the parameter p,

$$x_j(t) \leftarrow x_j(t)p. \tag{12}$$

This scaling results in short-term depression if $p < 1$ and short-term potentiation if $p > 1$. To ensure the maintenance of a sparse activity we implemented STD with $p = 0.6$ and $\tau_x = 150$ ms.

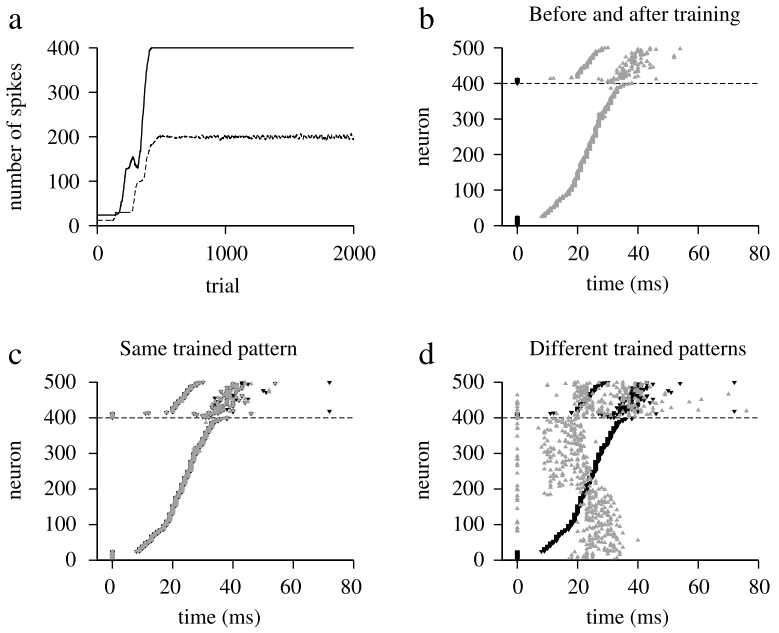

Fig. 1. Network response when two patterns are trained simultaneously. (a) Total number of spikes per trial. Excitatory neurons are represented by a continuous line, inhibitory neurons by a dotted line. The two patterns are presented alternately. (b)–(d) The superimposed rasterplots of two trials. Excitatory neurons are labeled from 1 to 400, while inhibitory ones from 401 to 500 (the dashed line separates both types of neurons). Neurons are ordered according to the first time they spike in one of the trials. (b): Network response induced by the same pattern before (black) and after (gray) training. The untrained pattern does not elicit any activity, and only the externally generated spikes are observed. After training the pattern elicits an activity for tenths of milliseconds. (c): Activity induced by the same initial pattern after training, in two distinct trials. The little fluctuation between the two rasterplots results from the synaptic modification in-between trials. Nevertheless, the spike times are similar, resulting in a correlation measure $C^{TT'} = 0.99$. (d): Rasterplots when two different trained patterns are presented after training. The network response is clearly different, which is confirmed by the correlation measure ($C^{TT'} = 0.037$).

3. Development of trajectories

We implemented the training protocol to evaluate the capacity of the network in different scenarios. We started with the simplest case, in which the number of sequences to be stored is two. Before the training, any initial condition results in very low activity (Fig. 1(a); between 1 and 100 trials), since all excitatory synaptic weights are initially weak. Therefore, in a naïve network, only the neurons directly forced to spike are activated, and the activity is not spread throughout the postsynaptic neurons (Fig. 1(b)). The network learns a pattern as it is induced throughout repetitive trials of stimulation. As the weight matrix is changed, the evoked activity tended to stabilize on the previously set spiking frequency A_{goal} (Fig. 1(a)). As patterns became trained, which took at least 500 trials, a feedforward path of strengthened connections was engraved in the network [35]. The network works as a spatiotemporal memory device, since when more than one pattern are trained simultaneously, it comes up with distinct responses to each one of them (Fig. 1(c) and (d)).

To evaluate the memory capacity of the system, we simulated the training of up to 30 patterns. In previous papers [24,25], the measurements were taken at roughly 1000 trials, which, in an overestimation (considering the length of 100 ms per trial), would correspond to approximately 100 s. Since the typical homeostatic scaling times are in the order of hours [36] or even days [29], and the simulations with large P took longer to converge, we analyzed the system through longer training periods (over 30 thousand trials, about 5 h).

4. Correlation measure

To compare the timing of excitatory action potentials we introduce the correlation measure $C^{TT'}$ between two trials T and T'. The correlation is analogue to a juxtaposition of the rasterplots with a Gaussian tolerance $\sigma = 1$ ms,

$$C^{TT'} = \frac{1}{\gamma} \sum_{i=1}^{N_e} \sum_{k=1}^{S_i^T} \exp\left[-\frac{\left(t_{i,k}^T - t_{i,l}^{T'}\right)^2}{2\sigma^2} \right], \tag{13}$$

where $t_{i,k}^T$ is the time of the kth spike of neuron i in trial T and l is the spike of neuron i fired in trial T' that is closest in time to $t_{i,k}^T$. Larger values of σ shift and flatten the curve upwards to $C = 1$, but do not introduce any additional information about

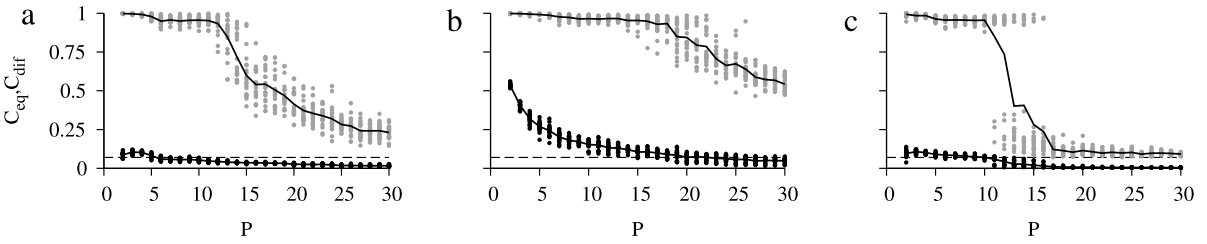

Fig. 2. Memory capacity of the network. (a) Mean correlation measurements according to the number of patterns trained simultaneously (P), between trials initiated with the same (C_{eq}; gray circles) or different (C_{dif}; black circles) patterns. Each point is calculated as the mean value of C between two successive presentations of the same pattern across 35 000 trials. The mean value is represented by a black line in each case. The dashed line represents the minimal correlation of two trials that share the same initial condition ($C = 0.07$) for comparisons. (b) Same as (a), but without weight limitation. (c) The same as in (a), but with $\alpha_A = 1$.

the system. The normalization γ is the largest value between the combined activity of the trials T and T' and its expected value $A_{goal}N_e$,

$$\gamma = MAX\left(\sum_{i=1}^{N_e} S_i^T, A_{goal}N_e\right). \tag{14}$$

The correlation value is low whether the spiking times are imprecise due to the exponential term, or unreliable due to the normalization term (γ), while it tends to unity if the two trials have similar spike times.

A quantitative analysis of the similarity between two responses to the same initial pattern is made with the average correlation measure C_{eq},

$$C_{eq} = \frac{1}{PN_T}\sum_{\mu=1}^{P}\sum_{T=T_i}^{T_f} C^{TT'}, \tag{15}$$

where P is the total number of patterns (different initial conditions) to be stored in the network, $\mu = 1, \ldots, P$ is the pattern index, and T_i and T_f represent the first and last trials, respectively, used to compute C, while T' is the previous trial (before T) with the same initial condition. $N_T = T_f - T_i$ is the total number of trials used to compute the correlation C. To verify if the patterns are being correctly discriminated, we also computed the mean value o $C^{TT'}$ in which T and T' are subsequent trials with different initial conditions. The activity correlation after presentation of two different patterns is given by

$$C_{dif} = \frac{1}{PN_T}\sum_{\mu=1}^{P}\sum_{T=T_i}^{T_f} C^{TT'}. \tag{16}$$

For C_{dif} the trial T' corresponds to the previous trial (before T) with a different initial condition. As the simulation goes on, the weights are updated at the end of each trial, the raster plots are registered and C is calculated.

As a consequence of increasing the number of trained patterns, we expect an impoverished quality of memory retrieval. This appears as a decrease in the average correlation measure C_{eq} (Fig. 2). If the spike times between two consecutive presentations of the same pattern do not match, the correlation value drops, which starts to happen when more than 12 patterns are trained simultaneously (Fig. 2(a)). Additionally, we tested the consequences of the hard bounds for excitatory synapses, simulating the system without any constrain for synaptic strength growth. The network capacity increases when hard bounds are eliminated (Fig. 2(b)). However, if the number of stored patterns is low, the correlation between the activities evoked by different trained patterns also increases (Fig. 2(b); $P < 10$). This means that for a small number of patterns, they tend to become mixed, mainly due to the activation of post-synaptic neurons by only a few presynaptic spikes.

5. Memory trace controls transition between learning modes

The activity trace is introduced to take into account a delay between the activity change and the synaptic scaling [27]. It is interesting to remark that it is a also a way of keeping memory of the neuronal activity throughout trials. We tested the limit of $\alpha_A = 1$, which corresponds to the absence of an activity trace delay, to see its effect on the network capacity. The correlation graph (Fig. 2(c)) shows not only a smaller capacity but also a region where pattern recognition is reached in part of events and not in others, suggesting a sharp transition with a coexistence region. Since the activity trace does not carry information between trials, the weights were always optimized to the last pattern presented, effectively forgetting the others.

It is also worthy to discuss the network capacity in terms of the distribution of weights, after a number of different patterns have been learned. This is shown in Fig. 3, for three different regimes: below maximum capacity, near maximum capacity

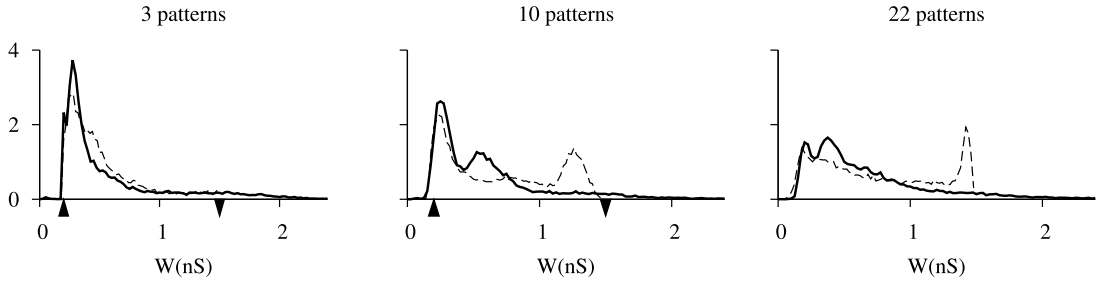

Fig. 3. Typical synaptic weight distributions of all the connections between excitatory neurons in a network after 47 000 trials. The number of trained patterns in each case were 3, 10 or 22 (see Fig. 2(a) and (b) for the mean C values), with and without weight limitation (dotted black and continuous gray lines, respectively). The arrowheads point to the initial value of $W_{exc\to exc} = 0.2$ nS (pointing upwards) and the maximum value in the bounded simulation (downwards).

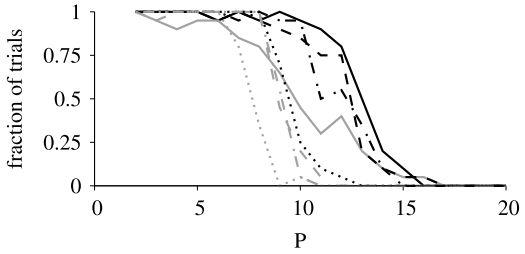

Fig. 4. Slow-decaying inhibitory connections boost the reproduction of spike time sequences. The curves show the fraction of trials in which the recovery is considered successful, i.e., $C > 0.9$, in function of the number of patterns being trained simultaneously in the network. There are four different inhibition configurations that are compared. These are, along with the regular configuration which features both $GABA_A$ and $GABA_B$ currents and fixed inhibitory weights (black continuous line), one with inactive inhibitory synapses ($W_{inh\to exc} = 0$; dotted gray), one with just $GABA_A$ current and doubled inhibitory weights (double dashed gray) and another with just a $GABA_B$ current (dashed black). Similarly, the contribution of the NMDA component was also tested in networks that lacked this component, with and without the inhibitory current with long decay (with $GABA_A$; continuous gray and dotted black, respectively) and without $GABA_A$ (dot-dashed black and dot-dashed gray).

and beyond maximum capacity, for both with and without weight limit W_{max}. In both cases, below the maximum capacity, the distribution has a peak at low values of W. For the bounded W_{max} case, that low W peak decreases and another peak appears just below W_{max} close to the maximum capacity. In the unbounded case the population at large W values increases, although it seems to be naturally limited at $W \approx 2.0$ nS. Also in this case, a second peak, above the starting weight value, develops. We guess that this is a natural trend of the unbounded learning dynamics: as the number of patterns increases, the weight distribution evolves to a unimodal one when following a weight dependent update rule [27]. The distribution peak at W_{max} observed in the bounded case would be a byproduct of the sharp bound, that would act as a trap. Beyond the maximum capacity regime, in both cases, the separate peak at small W vanishes, i.e., weights do not stay at the initial value. This means that the network can be trained whenever there are weights to be written on, which translates into less competition among the patterns and a larger capacity in the unbounded case.

6. Inhibition dynamics influences memory capacity

Based on the knowledge that inhibitory interactions have a huge significance to the precision of spike times [37,8,3], we examined the effects of each current component that presents different time scales (Fig. 4). For each value of P, 20 networks were simulated, and the measurements were performed after activity stabilization. Each curve represents the fraction of events that resulted in $C_{eq} > 0.9$. The AMPA component is needed for the initial development of activity, so it was kept unchanged. For a few trained patterns, the system works even in the absence of inhibition, but it is slightly more robust in the presence of a $GABA_A$ mediated inhibition. The inclusion of an excitatory current component with a longer time decay, such as the one mediated by NMDA receptors, generates a slightly longer response, which is more alike to *in vitro* [9]. However, in the network without inhibition the presence of NMDA current decreases the capacity.

When an inhibitory component with slow decay, namely a $GABA_B$ mediated one, is introduced, the capacity is greatly enhanced. If a balance between excitation and inhibition is adjusted by simply scaling the inhibitory synaptic weights, with only the $GABA_A$ component, the results are better than in the uninhibited case, but still poorer if compared to the ones in which $GABA_B$ is present. We conclude that $GABA_A$ does not alter the maximum capacity achievable, but only the reliability instead.

There is still a better result achieved with both inhibitory and excitatory components, each comprised of one of rapid and one of slow decay. Further modifications in the $GABA_B$ component amplitude did not effect a better performance (not

shown). If $GABA_B$ is present without an NMDA component the maximum number of patterns the network can learn is similar but the actual recovery is less reliable.

7. Conclusions

We studied neural networks with synaptic weights evolving under PSD synaptic scaling, that can be trained to generate a unique spike sequence to a given stimulus. In general lines, we follow the same setup as in Ref. [24], extending the results for much longer learning times and exploring effects of different balance conditions and learning parameters. With longer periods of learning, it was possible to achieve an even better performance, and in the absence of noise a maximum capacity was estimated.

The more patterns are trained at the same time, the higher is the competition among them for keeping their own set of potentiated connections. If the weights are unbounded, there is a larger available volume in the weight space, and therefore the competition is smaller, resulting in a larger capacity. Furthermore, in this case the distribution of weights for a large number of patterns is naturally limited, so it is not necessary to impose a sharp bound in the weight dynamics. Nevertheless, there is a compromise, since in this case correlations between patterns that do not depress each other increase. If the synaptic weights are bounded, in order to keep more trained patterns, different pathways percolating the network must be available, which translates into more recurrent connections [24].

We have also found that the presence of an inhibitory current with a longer decaying time makes the responses more precise. For this, a slow decaying inhibition, controlled by $GABA_B$ receptors, was introduced. Even in the absence of NMDA the network performs better, so it is not exactly about overall excitation and inhibition balance but more about the longer time scale. If not, the case in which the inhibition is compensated by increasing the $GABA_A$ component amplitude would also yield better results.

If the trace of activity encompasses a longer range of time, i.e. α_A is smaller, the network develops the capacity to keep simultaneous memories beyond the initial feedforward capacity. Therefore different trace dynamics promote different levels of ability to storage past stimuli (e.g. [38]). It has also been shown that a homeostasis activity detector needs to act in a comparable time scale to Hebbian plasticity in order to stabilize the system [39].

Some structural mechanisms used for the generation of precise spiking times, such as axonal delays [15] or columnar architecture [16], were not needed in this model, but it remains unknown how the system would respond if they are combined. This remains an interesting subject for further investigation. Additional modifications on the PSD synaptic scaling model are needed to achieve better stability, to avoid memory overwriting, and for the embedding of the spike patterns in a non-quiescent basal state.

Acknowledgments

The authors acknowledge the Brazilian funding agencies CNPq (141452/2010-2 and 235144/2014-2, for EJA, and 202183/2015-7 and 141412/2013-5, for BEPM), and the computational resources from Computational Physics Laboratory of the Physics Institute of Universidade Federal do Rio Grande do Sul (CPL-PI-UFRGS). There are no competing financial interests in the present work.

References

[1] M. Abeles, Corticonics: Neural Circuits of the Cerebral Cortex, Cambridge University Press, 1991.
[2] R. Brette, Philosophy of the spike: rate-based vs. spike-based theories of the brain, Front. Sys. Neurosci. 9 (2015) 151.
[3] S. Denève, C.K. Machens, Efficient codes and balanced networks, Nature Neurosci. 19 (2016) 375–382.
[4] E.J. Agnes, R. Erichsen Jr., L.G. Brunnet, Model architecture for associative memory in a neural network of spiking neurons, Physica A 391 (2012) 843–948.
[5] A. Litwin-Kumar, B. Doiron, Formation and maintenance of neuronal assemblies through synaptic plasticity, Nat. Comm. 5:5319 (2014) 1–12.
[6] F. Zenke, E.J. Agnes, W. Gerstner, Diverse synaptic plasticity mechanisms orchestrated to form and retrieve memories in spiking neural networks, Nat. Comm. 6:6922 (2015) 1–15.
[7] E.J. Agnes, R.E. Erichsen Jr., L.G. Brunnet, Associative memory in neuronal networks of spiking neurons: architecture and storage analysis, LNCS 7552 (2012) 145–152.
[8] P. Tiesinga, J.-M. Fellows, T.J. Sejnowski, Regulation of spike timing in visual cortical circuits, Nature Rev. Neurosci. 9 (2008) 97–109.
[9] D.V. Buonomano, Timing of neural responses in cortical organotipic slices, Proc. Natl. Acad. Sci. 100 (2003) 4897–4902.
[10] C. Kayser, N.L. Logothethis, S. Panzeri, Milisecond encoding precision of auditory cortex neurons, Proc. Natl. Acad. Sci. 107 (2010) 16976–16981.
[11] M. London, A. Roth, L. Beeren, M. Häusser, P. Latham, Sensitivity to perturbations *in vivo* implies high noise and suggests rate coding in cortex, Nature 466 (2010) 123–128.
[12] A. Luczak, B.L. McNaughton, K.D. Harris, Packet-based communication in the cortex, Nature Rev. Neurosci. 16 (2015) 745755.
[13] E.L. Bienenstock, A model of neocortex, Net. Comput. Neural Syst. 6 (1995) 179–224.
[14] M. Diesmann, M.-O. Gewaltig, A. Aertsen, Stable propagation of synchronous spiking in cortical neural networks, Nature 402 (1999) 529–533.
[15] E.M. Izhikevich, Polychronization: computation with spikes, Neur. Comp. 18 (2) (2006) 245–282.
[16] J.K. Jun, D.Z. Jin, Development of neural circuitry for precise temporal sequences through spontaneous activity, axon remodeling, and synaptic plasticity, PLoS One 2(8) (2007) 1–17.
[17] Y. Aviel, C. Mehring, M. Abeles, D. Horn, On embedding synfire chains in a balanced network, Neural Comput. 15(6) (2003) 1321–1340.
[18] N. Masuda, H. Kori, Formation of feedforward networks and frequency synchrony by spike-timing-dependent plasticity, J. Comput. Neurosci. 22 (2007) 327–345.

[19] A. Kumar, S. Rotter, A. Aertsen, Conditions for propagating synchronous spiking and asynchronous firing rates in a cortical network model, J. Neurosci. 28(20) (2008) 5268–5280.
[20] I.R. Fiete, W. Senn, C.Z.H. Wang, R.H.R. Hahnloser, Spike-time-dependent plasticity and heterosynaptic competition organize networks to produce long scale-free sequences of neural activity, Neuron 65 (2010) 563–576.
[21] S.O. Verduzco-Flores, M. Bodner, B. Ermentrout, A model for complex sequence learning and reproduction in neural populations, J. Comput. Neurosci. 32 (2012) 403–423.
[22] A. Waddington, P.A. Appleby, M.D. Kamps, N. Cohen, Triphasic spike-timing-dependent plasticity organizes networks to produce robust sequences of neural activity, Front. Comput. Neurosci. 6 (88) (2012) 1–14.
[23] C. Trengrove, C. van Leeuwen, M. Diesmann, High-capacity embedding of synfire chains in a cortical network model, J. Comput. Neurosci. 34 (2013) 185–209.
[24] J.K. Liu, D.V. Buonomano, Embedding multiple trajectories in simulated recurrent neural networks in a self-organizing manner, J. Neurosci. 29 (42) (2009) 13172–13181.
[25] J.K. Liu, Z.-S. She, A spike-timing pattern based neural network model for the study of memory dynamics, PLoS One 4 (7-e6247) (2009) 1–8.
[26] G.G. Turrigiano, K.R. Leslie, N.S. Desai, L.C. Rutherford, S.B. Nelson, Activity-dependent scaling of quantal amplitude in neocortical neurons, Nature 391 (1998) 892–896.
[27] M.C.W. van Rossum, G.-q. Bi, G.G. Turrigiano, Stable Hebbian learning from spike timing-dependent plasticity, J. Neurosci. 20 (23) (2000) 8812–8821.
[28] D.V. Buonomano, Learning rule for the emergence of stable dynamics and timing in recurrent networks, J. Neurophys. 94 (2005) 2275–2283.
[29] G.G. Turrigiano, Homeostatic synaptic plasticity: Local and global mechanisms for stabilizing neuronal function, Cold Spring Harb. Perspect. Biol. 4:a005736 (2012) 1–18.
[30] F. Fröhlich, M. Bazhenov, T.J. Sejnowski, Pathological effect of homeostatic synaptic scaling on network dynamics in diseases of the cortex, J. Neurosci. 28 (2008) 1709–1720.
[31] E.M. Izhikevich, Simple model of spiking neurons, IEEE Trans. Neural Netw. 14 (6) (2003) 1569–1572.
[32] E.M. Izhikevich, G.M. Edelman, Large scale model of mammalian thalamocortical systems, Proc. Natl. Acad. Sci. 105 (9) (2008) 3593–3598.
[33] E.M. Izhikevich, J.A. Gally, G.M. Edelman, Spike-timing dynamics of neuronal groups, Cerebral Cortex 14 (2004) 933–944.
[34] L.F. Abbott, S.B. Nelson, Synaptic plasticity: taming the beast, Nature Neurosci. 3 (2000) 1178–1183.
[35] D.V. Buonomano, W. Maass, State-dependent computation: spatiotemporal processing in cortical networks, Nature Neurosci. 10 (2009) 113–125.
[36] K. Ibata, Q. Sun, G.G. Turrigiano, Rapid synaptic scaling induced by changes in postsynaptic firing, Neuron 57 (2008) 819–826.
[37] M. Wehr, A.M. Zador, Balanced inhibition underlies tuning and sharpens spike timing in auditory cortex, Nature 426 (2003) 442–446.
[38] A. Pitas, A.L. Albarracn, M. Molano-Mazn, M. Maravall, Variable temporal integration of stimulus patterns in the mouse barrel cortex, Cerebral Cortex (2016). http://dx.doi.org/10.1093/cercor/bhw006.
[39] F. Zenke, G. Hennequin, W. Gerstner, Synaptic plasticity in neural networks needs homeostasis with a fast rate detector, PLoS Comput. Biol. 9 (11) (2013) e1003330.